





Optimization of Mechanical and Durability Properties of Manganese Slag Hybrid Fiber Concrete Using an L9 Orthogonal Design and Grey Relational Analysis

Feng Li^{1,2*} , Chee Khoo Ng¹ 

¹ Department of Civil Engineering, Faculty of Engineering, Universiti Malaysia Sarawak, Kota Samarahan 94300, Malaysia

² Faculty of Civil Engineering, Henan Institute of Engineering, Zhengzhou 451191, China

Corresponding Author Email: fengli@haue.edu.cn

Copyright: ©2025 The authors. This article is published by IETA and is licensed under the CC BY 4.0 license (<http://creativecommons.org/licenses/by/4.0/>).

<https://doi.org/10.18280/ijdne.200704>

ABSTRACT

Received: 28 June 2025

Revised: 23 July 2025

Accepted: 27 July 2025

Available online: 31 July 2025

Keywords:

manganese slag hybrid fiber concrete, mechanical properties, durability, optimal mix proportion, steel fiber, polypropylene fiber, grey relational analysis, L9 orthogonal experiment

Studies have highlighted manganese slag (MnS) mixed-fiber concrete as a construction material, in view of the effects of varying proportions of MnS, steel fibers (SF), and polypropylene fibers (PPF) on the mechanical properties and durability of C30 MnS hybrid fiber-reinforced concrete (MHFC). Using an L9 orthogonal design, ten mix ratios were tested for compressive strength, flexural strength, and chloride ion resistance at 7, 28, 56, and 91 days. A grey relational analysis (GRA) method was employed to comprehensively evaluate nine mix proportioning schemes across four curing ages. By analyzing the grey relational degrees, the optimal mix proportioning scheme was identified. Results indicated that SF had the greatest positive impact on both compressive and flexural strength, followed by MnS, while PPF had a limited effect. The optimal mix—20% MnS, 1.0% SF, and 0.5% PPF—achieved a 23% increase in compressive strength and 33% in flexural strength at 28 days. In terms of the durability of concrete in corrosive environments, the optimal performance was achieved with a mix proportion of 10% MnS, 1.0% SF, and 1.0% PPF. These findings provide guidance for optimizing MHFC and highlight the potential of industrial by-products in enhancing concrete durability. Further research is recommended to refine mix designs and assess long-term field performance.

1. INTRODUCTION

Concrete is a composite material composed of cement, fine aggregates, coarse aggregates, and water. Portland cement, a key ingredient in conventional concrete, functions as a binder that ensures the cohesion of aggregates within the mixture [1]. However, cement production is associated with significant environmental concerns due to its energy-intensive manufacturing process and substantial CO₂ emissions [2]. The calcination of limestone and the high-temperature clinkerization process in cement kilns contribute approximately 7–8% of global anthropogenic CO₂ emissions, making the development of alternative cementitious materials a critical research priority. For each ton of cement produced in 2020, approximately 0.59 tons of CO₂ were typically emitted [3]. Consequently, there is a growing emphasis on exploring supplementary cementitious materials (SCMs) that are energy-efficient and environmentally sustainable, while maintaining comparable or superior mechanical properties to Ordinary Portland Cement (OPC). One such promising SCM is manganese slag (MnS), an industrial by-product derived from the production of electrolytic manganese [4].

Electrolytic MnS is generated as a solid waste in filters following the sulfuric acid leaching of manganese carbonate ore, oxidative deferrization with MnO₂, and lime neutralization [5]. Recent studies have highlighted its potential

as an SCM due to its pozzolanic and latent hydraulic activity, which facilitates cement hydration and enhances concrete properties. Infrared spectroscopy and other experimental techniques have confirmed that MnS exhibits reactivity similar to natural pozzolanic materials, enabling its partial replacement of cement in concrete production [6]. MnS demonstrates both hydraulic and pozzolanic behavior, with a reactivity range lower than that of ground granulated blast furnace slag (GGBFS), but higher than that of fly ash. Its chemical composition, which includes CaSO₄·2H₂O, SiO₂, Al₂O₃, Fe₂O₃, and MnO₂, allows it to interact with cement hydration products, improving the microstructure and durability of hardened concrete [7]. It is found that calcium aluminate silicate hydrate (CASH) gel is also the hydration product of manganese slag cement slurry, except for calcium hydrate crystal and CSH gel [8]. The sulphate in the electrolytic manganese slag can react with the aluminum minerals in the concrete, effectively improving the volume stability. The dense concrete structure can effectively solidify the heavy metal ions in the electrolytic manganese slag [9]. The active Al₂O₃ component in GGBFS reacts with a sulphate activator to create Aft [10]. As a result, MnS has expanded beyond traditional low-value applications, such as road base material and aggregate substitution in bricks and blocks, and is now being considered for high-performance concrete applications [11]. MnS enhances marine concrete's sulfate

resistance: 30% replacement improved resistance by 33% after 180 days by densifying microstructure and reducing calcium hydroxide, though 40% replacement slightly decreased performance due to lower early strength [12]. High-temperature sintered MnS, possessing vitrified properties and high compressive strength, can be crushed and graded to serve as an aggregate substitute in concrete. Calcined MnS at 1100°C exhibits large grains and surface pores, with CaSO₄ particles identified via elemental mapping. These CaSO₄ particles enhance cement hydration by releasing SO₄²⁻ to form C-S-H gel with cement components, densifying the concrete microstructure and improving flexural strength [13]. This advancement aligns with sustainable construction practices by integrating industrial waste into concrete, reducing cement dependency, and lowering the carbon footprint of construction materials [14].

Despite its advantages, conventional concrete suffers from inherent limitations, including high compressive strength but low flexural and tensile strength, leading to brittleness and reduced durability under mechanical loads. To address these weaknesses, fibers and industrial by-products with pozzolanic activity are often incorporated into concrete mixtures to improve flexural strength and fracture toughness [15]. Concrete is classified as a quasi-brittle material, meaning it exhibits limited plastic deformation before failure. The addition of fibers enhances the material's toughness by bridging cracks and improving post-cracking behavior, thereby mitigating premature failure [16]. Among various fiber types, polypropylene fibers (PPF) are widely utilized due to their chemical stability in alkaline environments, availability, and cost-effectiveness. While PPF has a lower modulus of elasticity and strength compared to high-strength fibers such as steel, its ductility enables it to enhance the impact resistance and energy absorption capacity of concrete [17]. Research has demonstrated that incorporating PPF into concrete mixtures enhances stress resistance, fatigue life, thermal stability, and mechanical properties, particularly in applications requiring enhanced tensile and shear strength [18-20].

To further optimize concrete performance, hybrid fiber-reinforced systems have gained significant attention, as they combine fibers with different mechanical properties to achieve superior mechanical and durability characteristics. Low-modulus fibers such as polypropylene, polyamide, and basalt are commonly used to suppress early-age shrinkage cracks, improve resistance to temperature variations, and enhance concrete's resistance to microcracking under mechanical loads [21, 22]. Experimental findings indicate that PPF reinforcement improves the microstructural integrity of concrete by preventing the propagation of microcracks, thereby enhancing resistance to shrinkage, freeze-thaw cycles, and sulfate attack [23, 24]. Additionally, research on high-strength concrete reinforced with fibers has shown that fiber incorporation significantly increases fracture toughness, mitigates brittle failure, and effectively dissipates fracture energy [25-27]. Given that concrete is a multi-phase composite material, strategically combining different fiber types can optimize performance at the microscopic, mesoscopic, and macroscopic levels, contributing to enhanced mechanical properties and long-term durability.

Among fiber types, steel fibers (SF) are widely recognized for their ability to enhance both strength and toughness. Research has demonstrated that incorporating SF into concrete at volume fractions of 0.5%, 1.0%, 1.5%, and 2.0% leads to

significant improvements in compressive and flexural properties [28]. Experimental studies suggest that 1.5% SF reinforcement is optimal, yielding a compressive strength increase of approximately 15.3% while also significantly improving post-cracking strength and flexural ductility. The use of hybrid SF-PPF systems has been found to further enhance flexural properties, crack propagation resistance, and energy absorption capacity [29-31]. Comparative studies of fiber-reinforced concrete mixtures have shown that SF primarily enhances mechanical strength, while PPF contributes to improving toughness, durability, and resistance to environmental degradation [32, 33]. Additionally, the effect of PPF dosage on concrete performance under elevated temperatures indicates that incorporating 1 kg/m³ of fibers enhances heat resistance and residual strength, making fiber-reinforced concrete a viable material for extreme environmental conditions [18, 34].

Grey relational analysis (GRA) has been widely applied in material optimization studies, particularly for evaluating multi-factor performance in composite materials. Before pavement construction, the optimum asphalt content of hot mix asphalt (HMA) must be determined through mix design. A GRA-based algorithm was developed for HMA design optimization, where asphalt mixture specimens were comparatively tested to validate the algorithm's effectiveness [35]. Similarly, another study systematically investigated and optimized the influence of key parameters - specifically the ground granulated blast furnace slag replacement ratio - using grey relational analysis methodology [36]. The methodological framework provides a scientific basis for systematically evaluating the influence of various curing-age mix proportioning schemes on the overall performance of concrete. These applications demonstrate GRA's capability to handle complex multi-parameter optimization problems in material science.

This study systematically investigates the synergistic effects of MnS, SF, and PPF on MnS hybrid fiber-reinforced concrete (MHFC) through an integrated experimental and analytical approach. The research examines the influence of MnS-SF-PPF ratios on mechanical properties and durability indicators, establishes optimal mixture proportions using an L9 orthogonal experimental design coupled with grey relational analysis across multiple curing ages, and elucidates the microstructural mechanisms underlying performance enhancement, with particular focus on MnS's role as a supplementary cementitious material in pore structure refinement and calcium hydroxide reduction.

The findings provide an optimized mix design framework that enhances the mechanical properties and durability of concrete, while promoting MnS as a high-performance supplementary cementitious material. The framework reduces cement consumption and carbon dioxide emissions, and lowers production costs through industrial byproduct utilization. Furthermore, it provides practical solutions for offshore structures and chloride-rich environments, demonstrating both economic and environmental benefits for sustainable construction.

2. MATERIALS AND METHODS

Although MnS exhibits hydraulic and pozzolanic properties, it cannot be directly utilized as a cement replacement in concrete without prior treatment [37]. To

enhance its reactivity and cementitious behavior, various activation methods can be applied, including mechanical grinding, thermal activation, and modulation activation. Among these, mechanical grinding and thermal activation are classified as physical activation methods, whereas modulation activation is considered a chemical activation technique. In this study, mechanical grinding is employed as the physical activation method to improve the performance of MnS in MHFC applications. Additionally, the properties of MnS vary with its source and processing conditions, resulting in differences in performance.

2.1 Test raw materials

The MnS utilized in this experiment was sourced from Xingyang City, Henan Province, China. In its raw state, the MnS appears as a black, viscous solid. The finely ground MnS

is presented in Figure 1. The chemical composition of the MnS post-treatment is detailed in Table 1. Additionally, the specific surface area of the processed MnS was measured at 400 m²/kg.



Figure 1. Finely ground MnS

Table 1. Chemical composition of MnS powder

Compound	SiO ₂	SO ₃	CaO	Al ₂ O ₃	Fe ₂ O ₃	MnO	MgO	Other
Percentage (%)	40.84	21.90	13.54	9.37	4.00	3.21	2.45	4.69

The SF employed in this experiment consists of 20 mm corrugated SF, manufactured in Zhengzhou City, Henan Province, China. The fundamental parameters of the SF are presented in Table 2, while their morphological characteristics are illustrated in Figure 2.



Figure 2. Appearance and form of SF

Table 2. Basic parameters of SF

Material	Fiber Type	Standard (mm)	Density (g/cm ³)	Tensile Strength (MPa)
Steel fiber	Wave pattern	20	7.8	1200

Table 3. Basic parameters of PPF

Fiber Type	Standard (mm)	Density (g/m ³)	Ignite (°C)	Tensile Strength (MPa)
Fibrillated	9	0.91	580	460

The PPF utilized in this experiment is are 9 mm-long bundle of single-filar PPFs, manufactured in Xingyang City, Henan Province, China. The fundamental properties of the fibers are detailed in Table 3, while their appearance and morphological characteristics are depicted in Figure 3.

The cement used in this experiment was produced in Henan Province. The key performance parameters of the cement are presented in Table 4.

The mineral admixtures used in this experiment include Class I fly ash, supplied in Henan Province, with its key

properties detailed in Table 5. Additionally, Class S95 slag powder was utilized, which was produced by Zhengzhou New Material Company.



Figure 3. Appearance of PPF

Table 4. Basic properties of PO42.5 ordinary cement

Material	Specific Area (m ² /kg)	Loss on Ignition (%)	Compression Strength (MPa)	Bending Strength (MPa)
Cement	385	2.45	48.0	9.5

Table 5. Components of fly ash

Type	SiO ₂	Al ₂ O ₃	Fe ₂ O ₃	CaO	MgO	Loss
Content (%)	62.74	20.62	6.55	5.27	3.75	1.07

The ordinary coarse aggregates with a particle size of 5–20 mm and high-quality river sand with a fineness modulus of 2.6 (0–5 mm) were used as fine aggregates. Tap water from Zhengzhou City, Henan Province, served as the mixing water. A high-efficiency polycarboxylic acid-based water-reducing agent, also produced in Zhengzhou City, was employed, providing a water reduction rate of 20%.

2.2 Mix design

An orthogonal experiment is an efficient multi-factor and multi-level experimental design method [38]. It selects

representative test points from the comprehensive experiment through the principle of orthogonality to reduce the number of experiments, reduce costs, and ensure the reliability of the results [39]. This approach enables the identification of the primary and secondary effects of different factors on the experimental objectives, ultimately facilitating the determination of the optimal parameter combination.

This study explored the influence of MnS, SF, and PPF on the comprehensive performance of MHFC through an orthogonal test system, and selected three key influencing factors and their levels: mass percentage of MnS (M_{MnS} , 5%, 10%, 20%), volume percentage of SF (V_{SF} , 0.5%, 1%, 1.5%), and volume percentage of PPF (V_{PPF} , 0.5%, 1%, 2%). Based on the L9 (3^3) orthogonal table design, a 3-factor 3-level orthogonal test scheme was designed.

To investigate the influence of three factors — mass percentage of MnS (A: M_{MnS}), volume percentage of SF (B: V_{SF}), and volume percentage of PPF (C: V_{PPF}) — on the compressive strength, flexural strength, and chloride resistance of concrete specimens, range analysis and analysis

of variance (ANOVA) were conducted using the statistical software SPSS to identify the significant factors. The range (R) is used to reflect the degree of influence of each factor on the indicator. The larger the R value, the more significant the influence of that factor on the test results. Variance (S^2) measures the degree of dispersion of results at different levels of a given factor. By comparing the S^2 values of different factors, one can preliminarily judge and rank the influence of each factor on the test results.

A total of 9 groups of mixed proportions were prepared for comparative analysis of the performance of MHFC. The experimental design scheme is shown in Table 6. The experimental sample $MnS_{20}SF_1PPF_{0.5}$ follows a standardized naming convention where the subscripts indicate the material mix proportions: 20% M_{MnS} , 1% V_{SF} , and 0.5% V_{PPF} . This systematic labeling applies uniformly across all samples in the study, with numerical subscripts directly reflecting each mix proportion (e.g., $MnS_5SF_{0.5}PPF_{0.5}$ denotes 5% M_{MnS} , 0.5% V_{SF} , and 0.5 vol% V_{PPF}).

Table 6. Design of MHFC with MnS, SF, and PPF

Item	Group Number	MnS (%)	SF (%)	PPF (%)	Material Dosage (kg/m ³)					
					Cement	Fly ash	Sand	Cobble	Water	Water reducer
1	$MnS_5SF_{0.5}PPF_{0.5}$	5	0.5	0.5	247	86	663	1000	140	3
2	$MnS_5SF_1PPF_1$	5	1	1	247	86	663	940	140	3.5
3	$MnS_5SF_{1.5}PPF_2$	5	1.5	2	247	86	663	890	140	3.9
4	$MnS_{10}SF_{0.5}PPF_1$	10	0.5	1	234	86	663	1000	140	3
5	$MnS_{10}SF_1PPF_2$	10	1	2	234	86	663	940	140	3.5
6	$MnS_{10}SF_{1.5}PPF_{0.5}$	10	1.5	0.5	234	86	663	890	140	3.9
7	$MnS_{20}SF_{0.5}PPF_2$	20	0.5	2	208	86	663	1000	140	3
8	$MnS_{20}SF_1PPF_{0.5}$	20	1	0.5	208	86	663	940	140	3.5
9	$MnS_{20}SF_{1.5}PPF_1$	20	1.5	1	208	86	663	890	140	3.9

2.3 Preparing concrete

To ensure optimal dispersion and uniformity of SF and PPF, the following mixing process was implemented based on experimental and engineering validation. Sand, cement, MnS, and coarse aggregates were loaded into a planetary mixer and blended at 30–50 rpm for 1.5 minutes to homogenize the binder-aggregate matrix. SF and PPF were introduced in three batches via a vibrating sieve, followed by 2 minutes of mixing to prevent clustering. Water and admixtures were incrementally added at reduced speed (20–30 rpm) for 2 minutes until achieving a fiber-free agglomeration state, with total mixing time capped at 6 minutes to avoid fiber damage. Post-mixing, the MHFC mixture was cast into the corresponding molds, compacted on a vibration table, cured for 24 hours before demolding, and tested at designated ages.

The prepared concrete mixture was poured into pre-prepared plastic molds in three successive layers. Each layer was initially compacted manually to ensure uniform distribution, followed by vibration on a small vibration platform for 3 to 5 minutes to eliminate air voids and enhance compaction. Finally, excess concrete and cement mortar on the specimen surface were leveled and removed using a spatula to ensure a smooth and uniform surface. After casting, the concrete specimens were kept at room temperature in a shaded environment for 24 hours before being manually demolded. Subsequently, the specimens were transferred to a curing chamber maintained at a temperature of $20 \pm 3^\circ\text{C}$ and a relative humidity of 95%. The curing time is 7, 28, 56, and 91 days.

Standard test specimens were prepared for each mix ratio, including three $150 \times 150 \times 150$ mm cubes for compressive strength, three $150 \times 150 \times 750$ mm beams for flexural strength, and three $\Phi 100 \times 50$ mm cylinders for chloride resistance, enabling a comprehensive evaluation of the concrete's performance under different mix designs. The test used a YAW-4306 microcomputer-controlled, fully automatic pressure testing machine for concrete strength testing and a HAD-MDTL chloride ion tester for electrical flux testing. The compressive and flexural strength tests were conducted according to the guidelines of BS EN 12390-3:2019 and BS EN 12390-5:2019 standards. This thesis employs the rapid chloride permeability test (electric flux method) in accordance with ASTM C1202, Standard Test Method for Electrical Indication of Concrete's Ability to Resist Chloride Ion Penetration.

2.4 Grey relational analysis

Grey relational analysis is a multivariate statistical method based on limited information, which can be used to reveal the correlation between multiple target variables [40]. This method has been successfully applied in multiple engineering fields such as urban spatial planning and Sustainable machining of grade 3 titanium alloys [41, 42]. The core principle is to establish the correlation between sequences by calculating the geometric proximity between the comparison sequence and the reference sequence, and ultimately quantifying it as the grey correlation degree. The grey

correlation degree serves as a quantitative indicator, where higher values correspond to better overall performance of the parameter combination.

Based on the theory of grey relational analysis, this study considers 36 sets of MHFC samples as a grey system. Based on the performance of the material at four different age periods of 7 days, 28 days, 56 days, and 91 days, the experimental data were divided into four independent analysis groups. In each analysis group, the optimal values of each performance indicator are selected to construct a reference sequence X_0 as the ideal trait, and the comprehensive performance data of 9 sets of MHFC specimens in this group are used as the comparison sequence X_i ($i=1, 2, 3, \dots, 9$). By calculating the geometric proximity between the sequences, the correlation degree between the performance of each set of specimens and the ideal trait is quantitatively evaluated, and the grey correlation degree evaluation index is finally obtained.

Step 1: The original experimental data is normalized, and the extreme value is normalized to eliminate the influence of dimensions. Extreme value normalization is calculated using the following formula.

For indicators where "higher values are better" (e.g., F_c and F_r), the formula is:

$$x'_i = \frac{x_i - \min(x)}{\max(x) - \min(x)} \quad (1)$$

where x_i is the original experimental data value for the i -th sample or parameter, and x'_i is the normalized value of x_i after dimensionless processing.

For indicators where "smaller values are better" (e.g., Q), the formula is:

$$x'_i = \frac{\max(x) - x_i}{\max(x) - \min(x)} \quad (2)$$

Step 2: Compare the comparative sequences with the reference sequence.

$$\Delta_i(k) = |x'_i(k) - x'_0(k)| \quad (3)$$

where, $\Delta_i(k)$ is the absolute difference between the

normalized comparative sequence $x'_i(k)$ and reference sequence $x'_0(k)$ at point k .

Step 3: Calculate the grey relational coefficients ($\xi_i(k)$).

$$\xi_i(k) = \frac{\min_i \min_k \Delta_i(k) + \rho \times \max_i \max_k \Delta_i(k)}{\Delta_i(k) + \rho \times \max_i \max_k \Delta_i(k)} \quad (4)$$

where, ρ is the distinguishing coefficient (typically $\rho=0.5$).

Step 4: Compute the grey relational degree (λ_i).

$$\lambda_i = \frac{1}{n} \sum_{k=1}^n \xi_i(k) \quad (5)$$

By computing the grey relational degrees between individual parameters and the integrated performance of MHFC using the described methodology, subsequent ranking of these values reveals the relative strength of association between each factor and MHFC performance. This ordered ranking effectively quantifies the sensitivity of each influencing parameter to the overall MHFC properties.

3. RESULT AND DISCUSSION

3.1 Test results of specimens

The test specimens were subjected to MHFC strength tests and chloride ion flux tests under standard conditions. with their compressive strength (F_c), flexural strength (F_r), and flux (Q) shown in Table 7. Specifically, F_{c7} denotes the compressive strength of concrete at 7 days of age (unit: MPa), F_{r28} denotes the flexural strength at 28 days of age (unit: MPa), and Q_{56} denotes the flux at 56 days of age (unit: Coulomb). The meanings of other symbols are similar.

The ANOVA results for the three factors— M_{MnS} (A), V_{SF} (B), and V_{PPF} (C)—at curing ages of 7, 28, 56, and 91 days are presented in Tables 8 to 10. In these tables, k_1 , k_2 , and k_3 represent the sum of test results at levels 1, 2, and 3 of each factor, respectively; μ_1 , μ_2 , and μ_3 are their corresponding mean values. R denotes the range, and S^2 is the variance.

Table 7. Test results of MHFC specimens at 7d, 28d, 56d, and 91d

Group Number	F_{c7} (MPa)	F_{r7} (MPa)	Q_7 (C)	F_{c28} (MPa)	F_{r28} (MPa)	Q_{28} (C)	F_{c56} (MPa)	F_{r56} (MPa)	Q_{56} (C)	F_{c91} (MPa)	F_{r91} (MPa)	Q_{91} (C)
MnS ₅ SF _{0.5} PPF _{0.5}	31.27	4.06	804	40.21	5.18	897	42.89	5.57	683	43.78	5.6	754
MnS ₅ SF ₁ PPF ₁	34.45	4.43	651	44.3	6.21	673	47.25	6.14	512	48.24	6.17	538
MnS ₅ SF _{1.5} PPF ₂	33.15	4.31	794	42.62	5.73	814	45.46	5.91	654	46.41	5.95	719
MnS ₁₀ SF _{0.5} PPF ₁	33.06	4.28	683	42.51	5.67	695	45.34	5.89	427	46.29	5.93	434
MnS ₁₀ SF ₁ PPF ₂	35.32	4.59	479	45.4	6.04	489	48.43	6.3	303	49.43	6.32	317
MnS ₁₀ SF _{1.5} PPF _{0.5}	34.35	4.64	637	44.17	5.98	651	47.11	6.11	409	48.1	6.14	396
MnS ₂₀ SF _{0.5} PPF ₂	33.6	4.33	456	43.2	5.23	548	46.08	5.99	329	47.04	6.02	418
MnS ₂₀ SF ₁ PPF _{0.5}	36.19	5.01	271	46.53	6.31	367	49.63	6.42	275	50.67	6.48	355
MnS ₂₀ SF _{1.5} PPF ₁	34.8	4.87	575	44.74	6.24	624	47.73	6.21	338	48.72	6.23	407

3.2 Range and variance analysis of compressive strength at different ages

According to the data analysis in Table 8, the addition of MnS, SF, and PPF significantly influences the compressive strength of MHFC, albeit to varying degrees compared to the control group. Range and variance analyses indicate that the order of influence on compressive strength is as follows: V_{SF}

(B) > M_{MnS} (A) > V_{PPF} (C). This suggests that steel fiber has the most pronounced effect on enhancing compressive strength, followed by MnS, while PPF has the least impact.

The results show that the compressive strength of conventional concrete without MnS and fiber at 28 days is 35.88 MPa, meeting the C30 strength requirement. A closer examination of the data reveals that, with an M_{MnS} of 10%, the compressive strength of the specimens initially increases and

then decreases as the V_{SF} rises. Specifically, as the V_{SF} increases from 0.5% to 1.0% and then to 1.5%, the compressive strength improves from 35.88 MPa to 40.21 MPa, 44.30 MPa, and 42.62 MPa, respectively—representing

increases of 12%, 23%, and 18% compared to ordinary concrete. This indicates the presence of an optimal V_{SF} , beyond which excessive fiber addition may result in diminishing returns in strength enhancement.

Table 8. Range and variance of the MHFC compressive strength at 7d, 28d, 56d, and 91d

	F_{c7}			F_{c28}			F_{c56}			F_{c91}		
	A	B	C	A	B	C	A	B	C	A	B	C
k_1	98.87	97.93	101.81	127.13	125.92	130.91	135.6	134.31	139.63	138.43	137.11	142.55
k_2	102.73	105.96	102.31	132.08	136.23	131.55	140.88	145.31	140.32	143.82	148.34	143.25
k_3	104.59	102.3	102.07	134.47	131.53	131.22	143.44	140.3	139.97	146.43	143.23	142.88
μ_1	32.96	32.64	33.94	42.38	41.97	43.64	45.2	44.77	46.54	46.14	45.7	47.52
μ_2	34.24	35.32	34.1	44.03	45.41	43.85	46.96	48.44	46.77	47.94	49.45	47.75
μ_3	34.86	34.1	34.02	44.82	43.84	43.74	47.81	46.77	46.66	48.81	47.74	47.63
R	1.9	2.68	0.16	2.44	3.44	0.21	2.61	3.67	0.23	2.67	3.75	0.23
S^2	0.63	1.2	0.004	1.03	1.98	0.06	1.18	2.25	0.009	1.24	2.35	0.009

Furthermore, the compressive strength of specimens increases with higher MnS content, reaching its maximum value at 20% MnS replacement. Similarly, increasing the SF content initially enhances compressive strength, peaking at 1.0% SF, beyond which a decline is observed. In contrast, PPF has only a marginal effect on compressive strength enhancement. Additionally, the most significant strength gain occurs between 7 and 28 days, while the increase from 56 to 91 days is comparatively minor. This suggests that the mechanical properties of the MHFC tend to stabilize over time as hydration and pozzolanic reactions progress.

The observed improvements in compressive strength can be attributed to the synergistic interaction between MnS and hybrid fibers, which together form a stable internal network structure within the MHFC matrix. The incorporation of SF and PPF enhances the bond between the aggregates and cement, thereby improving resistance to shear stress and inhibiting crack development. This reinforcement mechanism contributes to enhanced mechanical performance by hindering crack propagation and increasing overall structural integrity. However, when the fiber dosage exceeds a critical threshold, inadequate dispersion within the matrix may lead to fiber clumping. This results in inhomogeneous stress distribution, disruption of internal structural stability, and ultimately, a reduction in compressive strength. The findings highlight the importance of optimizing the proportions of MnS and fiber content to maximize compressive strength. Achieving a proper balance in the mix design ensures the formation of an interconnected and stable microstructure, prevents excessive fiber clustering, and maintains structural performance. These results provide valuable insights into the mechanical behavior of MHFC, offering guidance for future research and practical applications in sustainable construction materials.

3.3 Range and variance analysis of flexural strength at different ages

The experimental results in Table 9 indicate that incorporating MnS, SF, and PPF enhances the flexural strength of MHFC to varying degrees. Range and variance analyses reveal that the influence of the factors ranks in the following order: V_{SF} (B) > M_{MnS} (A) > V_{PPF} (C). This highlights that V_{SF} has the most significant effect on improving flexural strength, followed by M_{MnS} , while V_{PPF} exhibits a comparatively weaker impact.

Data analysis further demonstrates that the introduction of MnS and mixed fibers into C30 concrete generally enhances the flexural strength of the specimens compared to the baseline group, although the extent of improvement varies. At 7 days of age, the flexural strength of the fiber control group was recorded at 4.64 MPa. Both MnS and fiber reinforcement were found to improve flexural strength, with the degree of enhancement depending on fiber content. As the SF volume fraction increased from 0.5% to 1.0%, the flexural strength of the specimens improved by 11% and 33%, respectively. However, when the SF content was further increased to 1.5%, the flexural strength increment dropped to 23%, suggesting the existence of an optimal fiber content beyond which additional reinforcement yields diminishing returns. The results indicate that flexural strength initially increases and then declines with rising SF content, reaching a peak at 1.0%. In contrast, increasing the PPF content from 0.5% to 2.0% does not result in a significant enhancement in flexural strength, reaffirming the relatively limited contribution of PPF to this property. Additionally, the increase in flexural strength from 7 to 28 days is more pronounced than the increment observed from 56 to 91 days, suggesting that the mechanical properties tend to stabilize over time as the material continues to mature.

Table 9. Range and variance of the MHFC flexural strength at 7d, 28d, 56d, and 91d

	F_{r7}			F_{r28}			F_{r56}			F_{r91}		
	A	B	C	A	B	C	A	B	C	A	B	C
k_1	12.8	12.67	13.71	17.12	16.08	17.47	17.62	17.45	18.1	17.72	17.55	18.22
k_2	13.51	14.03	13.58	17.69	18.56	18.12	18.3	18.86	18.24	18.39	18.97	18.33
k_3	14.21	13.82	13.23	17.78	17.95	17	18.62	18.23	18.2	18.73	18.32	18.29
μ_1	4.27	4.22	4.57	5.71	5.36	5.82	5.87	5.82	6.03	5.91	5.85	6.07
μ_2	4.5	4.68	4.53	5.9	6.19	6.04	6.1	6.29	6.08	6.13	6.32	6.11
μ_3	4.74	4.61	4.41	5.92	5.98	5.67	6.21	6.08	6.07	6.24	6.11	6.1
R	0.47	0.46	0.16	0.21	0.83	0.37	0.34	0.47	0.05	0.33	0.47	0.04
S^2	0.037	0.041	0.005	0.009	0.124	0.023	0.02	0.037	0.001	0.019	0.037	0.001

The observed improvement in flexural strength can be attributed to the formation of a micro-reinforcement network within the matrix, facilitated by the uniform dispersion of MnS and hybrid fibers. This network enhances the internal microstructure, mitigates crack initiation and propagation, and ultimately strengthens the concrete matrix. Steel fibers play a critical role in reinforcing weak zones within the specimens due to their high shear resistance, which effectively improves structural integrity and further enhances flexural strength. These findings underscore the importance of optimizing fiber content to maximize the flexural performance of MHFC.

3.4 Range and variance analysis of the electric flux of chloride ion corrosion in MHFC at different ages

Through range and variance analysis in Table 10, the influencing factors on the electric flux of MHFC are ranked in the order: M_{MnS} (A) > V_{SF} (B) > V_{PPF} (C). It indicates that the incorporation of MnS and fibers into the MHFC matrix contributes to a reduction in electric flux, thereby enhancing resistance to chloride ion penetration.

In detail, M_{MnS} consistently plays a dominant role in enhancing the chloride ion penetration resistance of MHFC, as evidenced by its significantly higher R and S^2 values compared to other factors, indicating a strong and stable influence. V_{SF} shows a relatively obvious promoting effect at early curing ages, but its effect gradually weakens as the curing age extends. However, once the V_{SF} surpasses a certain threshold, the electric flux begins to increase, indicating a decline in chloride ion resistance. For instance, at 28 days of curing, when the M_{MnS} remains constant at 10%, increasing the SF content from 0.5% to 1.0% results in a 24% reduction in electric flux. However, when the V_{SF} is further increased from 1.0% to 1.5%, the electric flux increases by 17%, leading to a drop in chloride ion penetration resistance from Q-II to Q-I classification. In contrast, V_{PPF} had a weaker effect at all ages, with consistently lower R values and S^2 values. Furthermore, as the curing age increases, the electric flux values gradually decline, indicating a continuous improvement in chloride resistance. The reduction in electric flux from 7 days to 28 days is more pronounced than the reduction observed between 56 days and 91 days, suggesting that the MHFC structure stabilizes over time.

Table 10. Range and variance of the MHFC chloride ion flux at 7d, 28d, 56d, and 91d

	Q ₇			Q ₂₈			Q ₅₆			Q ₉₁		
	A	B	C	A	B	C	A	B	C	A	B	C
k ₁	2249	1943	1712	2384	2140	1915	1849	1439	1367	2011	1606	1505
k ₂	1799	1401	1909	1835	1529	1992	1139	1090	1277	1147	1210	1379
k ₃	1302	2006	1729	1539	2089	1851	942	1401	1286	1180	1522	1454
μ ₁	749.7	647.7	570.7	794.7	713.3	638.3	616.3	479.7	455.7	670.3	535.3	501.7
μ ₂	599.7	467	636.3	611.7	509.7	664	379.7	363.3	425.7	382.3	403.3	459.7
μ ₃	434	668.7	576.3	513	696.3	617	314	467	428.7	393.3	507.3	484.7
R	315.7	201.7	65.6	281.7	203.6	47	302.3	116.4	27	288	132	42
S ²	16600	8200	2600	13600	8500	400	16900	2700	100	17800	3200	300

3.5 Grey relational analysis of NHFC comprehensive performance at different ages

A grey relational analysis was conducted on 36 sets of experimental data for NHFC at 7, 28, 56, and 91 days. For each curing age, the 9 experimental datasets were treated as an independent grey system. The optimal values within each system were designated as the ideal reference sequence (X_0), representing the target performance, while the remaining experimental data served as comparison sequences (X_i). After the data were normalized, gray correlation analysis was performed. The correlation coefficients and correlation degrees were calculated using formulas (1)-(5), and the correlation degrees of the four age stages were ranked separately. The results of the gray correlation analysis are shown in Tables 11-14.

Table 11 provided the results for NHFC at 7 curing ages. The $MnS_{20}SF_1PPF_{0.5}$ group achieved the highest grey relational grade (GRG) of 0.618, indicating superior early-age performance due to its optimal combination of 20% manganese slag (MnS_{20}), 1% silica fume (SF_1), and 0.5% polypropylene fiber ($PPF_{0.5}$). In contrast, $MnS_5SF_{0.5}PPF_{0.5}$ ranked lowest (GRG: 0.346), suggesting that low slag and silica fume content hinder early strength development. Notably, flexural strength (F_f) and compressive strength (F_c)

had higher correlation coefficients than Q (e.g., workability or permeability), emphasizing mechanical properties as critical for early performance.

In Table 12, $MnS_{20}SF_1PPF_{0.5}$ maintained dominance (GRG: 0.781), with its GRG increasing by 26.4% from 7 to 28 days, highlighting rapid strength gain. The $MnS_{10}SF_1PPF_2$ group (GRG: 0.657) emerged as a strong alternative, suggesting that higher fiber content (PPF_2) compensates for reduced slag (MnS_{10}). The lowest-performing group, $MnS_5SF_{0.5}PPF_{0.5}$ (GRG: 0.432), further validated that 5% slag inadequately supports mid-term hydration.

From Table 13, it can be seen that $MnS_{20}SF_1PPF_{0.5}$ achieved near-perfect alignment with ideal properties (GRG: 0.948), while $MnS_{10}SF_1PPF_2$ (GRG: 0.863) demonstrated diminishing returns from PPF_2 , implying fiber dosages beyond 0.5% offer marginal benefits. The $MnS_5SF_{0.5}PPF_{0.5}$ group (GRG: 0.519) remained the weakest, reinforcing that low slag and silica fume content limit long-term durability.

Table 14 provided that $MnS_{20}SF_1PPF_{0.5}$ (GRG: 0.929) and $MnS_{10}SF_1PPF_2$ (GRG: 0.881) exhibited sustained excellence, but $MnS_{20}SF_{1.5}PPF_1$ (GRG: 0.786) underperformed, indicating excessive silica fume ($SF_{1.5}$) may reduce long-term efficacy. The consistent poor performance of MnS_5 groups across all ages suggests that $\geq 10\%$ slag is essential for viable NHFC formulations.

Table 11. GRA of 7-Day MHFC Properties

Group Number	Grey Relational Coefficient			Grey Relational Grade	Rank
	F _c	F _r	Q	λ	
MnS ₅ SF _{0.5} PPF _{0.5}	0.333	0.333	0.370	0.346	9
MnS ₅ SF ₁ PPF ₁	0.374	0.371	0.452	0.399	6
MnS ₅ SF _{1.5} PPF ₂	0.356	0.358	0.374	0.363	8
MnS ₁₀ SF _{0.5} PPF ₁	0.355	0.355	0.432	0.381	7
MnS ₁₀ SF ₁ PPF ₂	0.387	0.390	0.601	0.459	2
MnS ₁₀ SF _{1.5} PPF _{0.5}	0.373	0.397	0.461	0.410	5
MnS ₂₀ SF _{0.5} PPF ₂	0.362	0.360	0.629	0.450	3
MnS ₂₀ SF ₁ PPF _{0.5}	0.401	0.451	1.000	0.618	1
MnS ₂₀ SF _{1.5} PPF ₁	0.379	0.429	0.507	0.439	4

Table 12. GRA of 28-Day MHFC Properties

Group Number	Grey Relational Coefficient			Grey Relational Grade	Rank
	F _c	F _r	Q	λ	
MnS ₅ SF _{0.5} PPF _{0.5}	0.481	0.482	0.333	0.432	9
MnS ₅ SF ₁ PPF ₁	0.604	0.818	0.438	0.620	4
MnS ₅ SF _{1.5} PPF ₂	0.546	0.617	0.366	0.510	8
MnS ₁₀ SF _{0.5} PPF ₁	0.543	0.599	0.425	0.522	7
MnS ₁₀ SF ₁ PPF ₂	0.648	0.733	0.589	0.657	2
MnS ₁₀ SF _{1.5} PPF _{0.5}	0.599	0.708	0.452	0.586	5
MnS ₂₀ SF _{0.5} PPF ₂	0.565	0.492	0.531	0.529	6
MnS ₂₀ SF ₁ PPF _{0.5}	0.701	0.877	0.765	0.781	1
MnS ₂₀ SF _{1.5} PPF ₁	0.621	0.834	0.470	0.642	3

Table 13. GRA of 56-Day MHFC Properties

Group Number	Grey Relational Coefficient			Grey Relational Grade	Rank
	F _c	F _r	Q	λ	
MnS ₅ SF _{0.5} PPF _{0.5}	0.555	0.571	0.432	0.519	9
MnS ₅ SF ₁ PPF ₁	0.739	0.781	0.565	0.695	6
MnS ₅ SF _{1.5} PPF ₂	0.651	0.680	0.450	0.593	8
MnS ₁₀ SF _{0.5} PPF ₁	0.645	0.672	0.667	0.662	7
MnS ₁₀ SF ₁ PPF ₂	0.812	0.871	0.907	0.863	2
MnS ₁₀ SF _{1.5} PPF _{0.5}	0.732	0.766	0.694	0.730	5
MnS ₂₀ SF _{0.5} PPF ₂	0.679	0.712	0.844	0.745	4
MnS ₂₀ SF ₁ PPF _{0.5}	0.903	0.953	0.987	0.948	1
MnS ₂₀ SF _{1.5} PPF ₁	0.767	0.818	0.824	0.803	3

Table 14. GRA of 91-Day MHFC Properties

Group Number	Grey Relational Coefficient			Grey Relational Grade	Rank
	F _c	F _r	Q	λ	
MnS ₅ SF _{0.5} PPF _{0.5}	0.585	0.579	0.393	0.519	9
MnS ₅ SF ₁ PPF ₁	0.800	0.796	0.540	0.712	5
MnS ₅ SF _{1.5} PPF ₂	0.695	0.695	0.411	0.601	8
MnS ₁₀ SF _{0.5} PPF ₁	0.689	0.688	0.658	0.678	7
MnS ₁₀ SF ₁ PPF ₂	0.887	0.883	0.872	0.881	2
MnS ₁₀ SF _{1.5} PPF _{0.5}	0.791	0.781	0.715	0.762	4
MnS ₂₀ SF _{0.5} PPF ₂	0.728	0.725	0.680	0.711	6
MnS ₂₀ SF ₁ PPF _{0.5}	1.000	1.000	0.788	0.929	1
MnS ₂₀ SF _{1.5} PPF ₁	0.833	0.829	0.697	0.786	3

3.6 Discussion

The grey relational analysis identifies MnS₂₀SF₁PPF_{0.5} as the optimal NHFC mix, exhibiting consistently high GRG at 7–91 days (Tables 11–14), with exceptional synergy between compressive/flexural strength (F_c/F_r) and durability (Q). This result is corroborated by orthogonal analysis, confirming its reliability for material design.

The observed trend can be attributed to three primary mechanisms. First, MnS generates a dense C-S-H gel through the pozzolanic reaction, enhancing hydration efficiency and

producing an interconnected, compact network of C-S-H gel. The interaction between C-S-H gel and secondary hydration products (e.g., ettringite) further improves microstructural integrity. Concurrently, Ca(OH)₂ crystals become less pronounced, indicating that the pozzolanic reaction between MnS and cement effectively consumes free Ca(OH)₂, thereby optimizing the pore structure of concrete and enhancing its resistance to chloride ion penetration. SF reduces chloride ion intrusion pathways by bridging microcracks and inhibiting crack propagation in the early stages, but its long-term effectiveness may be limited by the stability of the interface

between the fibers and the matrix. PPF, however, has a low elastic modulus and weak interaction with the matrix, resulting in a negligible improvement in resistance to chloride ion penetration. Secondly, MnS and hybrid fibers contribute to modifying the internal pore structure distribution within the MHFC, thereby enhancing durability. Thirdly, these materials actively absorb the cement hydration product $\text{Ca}(\text{OH})_2$, leading to a gradual decrease in the concentrations of Ca^{2+} and OH^- ions within the matrix. This reduction in ion concentration subsequently lowers the overall conductivity of the MHFC, resulting in a progressive decrease in electric flux values. However, with excessive fiber content, localized fiber accumulation can lead to fiber clustering, promoting microcrack formation, which adversely affects chloride ion resistance. The most significant reduction in electric flux occurs between 7 and 28 days, coinciding with the strongest absorption effect of $\text{Ca}(\text{OH})_2$ by MnS and fibers. In contrast, the reduction observed from 56 to 91 days is comparatively smaller, reflecting a more stabilized phase of hydration and microstructural development.

From an engineering application perspective, it is recommended that the M_{MnS} be controlled between 10-20% to ensure the long-term durability of concrete. V_{SF} should be increased in dosage (1.0-1.5%) during the early age stage (7-28 days) and appropriately reduced (0.5-1.0%) in the later stage (56-91 days) to achieve a balance between performance and cost. V_{PPF} can be reduced or omitted. In chloride-ion corrosive environments, special attention should be paid to the synergistic effect of manganese slag and steel fibers during the early stage (7-28 days), while ensuring that the manganese slag content serves as the core parameter for controlling the concrete's long-term resistance to chloride ions.

Based on the experimental results and systematic comparisons with similar studies, it is recommended to control the MnS content between 10-20% to ensure long-term concrete durability, while dynamically adjusting SF dosage (1.0-1.5% at 7-28 days, reduced to 0.5-1.0% at 56-91 days) for cost-performance balance, and minimizing or omitting PPF. Early-stage MnS-SF synergy is critical for chloride resistance, supported by slag-fiber studies. The MnS range aligns with cementitious mechanisms, while PPF reduction contrasts with some findings (e.g., 0.5% PPF benefits), likely due to hybrid-system interactions. Future work will integrate SEM/XRD to validate MnS-SF interface mechanisms, extending the macro-scale findings presented here.

4. CONCLUSIONS

Through the mechanical and durability experiments of MHFC, the range and variance analysis showed that the influencing factors on the mechanical properties of MHFC, from strongest to weakest, are SF content, MnS content, and PPF content. The factors influencing the durability performance of MHFC, from strongest to weakest, are MnS content, SF content, and PPF content. MnS and mixed fibers can significantly improve the mechanical properties of cement-based materials. The compressive strength at 28 days increases by up to 23%, and the flexural strength increases by up to 33% compared to the baseline group. The amount of MnS and SF affects the performance of MHFC. There is a particularly significant impact of MnS and steel fiber, while the impact of PPF is not significant enough. MnS significantly improves the resistance to chloride ion erosion, with 10%

MnS, 1.0% SF, and 1.0% PPF showing better resistance to chloride ion erosion. Therefore, MHFC with this proportion is strongly recommended for chloride-rich marine and coastal environments, including offshore wind turbine foundations, port structures, and bridge piers. As the curing age increases, the chloride ion erosion electric flux gradually decreases, while the compressive strength and flexural strength of MHFC gradually increase. This trend is most noticeable in the early stages of the test, particularly between 7 and 28 days. Considering both the improvement effect and economic rationality, the optimal mix ratio is when the content of MnS, SF, and PPF in MHFC is 20%, 1.0%, and 0.5%. From the perspectives of cost and environmental protection, MHFC, with this optimized proportion, reduces cement use by 70-100 kg/m^3 (cutting 63-85 $\text{kg CO}_2/\text{m}^3$), saves 3-7% of costs post-fiber reinforcement, and enables industrial waste valorization with carbon trading potential, demonstrating scalable sustainability.

REFERENCES

- [1] Rashad, A.M. (2014). A comprehensive overview about the influence of different admixtures and additives on the properties of alkali-activated fly ash. *Materials & Design*, 53: 1005-1025. <https://doi.org/10.1016/j.matdes.2013.07.074>
- [2] Miller, S.A. (2021). The role of data variability and uncertainty in the probability of mitigating environmental impacts from cement and concrete. *Environmental Research Letters*, 16(5): 054053. <https://doi.org/10.1088/1748-9326/abe677>
- [3] Benhelal, E., Zahedi, G., Shamsaei, E., Bahadori, A. (2013). Global strategies and potentials to curb CO_2 emissions in cement industry. *Journal of Cleaner Production*, 51: 142-161. <https://doi.org/10.1016/j.jclepro.2012.10.049>
- [4] Habert, G. (2013). Environmental impact of Portland cement production. In *Eco-Efficient Concrete*, pp. 3-25. <https://doi.org/10.1533/9780857098993.1.3>
- [5] Wang, J., Peng, B., Chai, L., Zhang, Q., Liu, Q. (2013). Preparation of electrolytic manganese residue-ground granulated blastfurnace slag cement. *Powder Technology*, 241: 12-18. <https://doi.org/10.1016/j.powtec.2013.03.003>
- [6] Allahverdi, A., Ahmadnezhad, S. (2014). Mechanical activation of silicomanganese slag and its influence on the properties of Portland slag cement. *Powder Technology*, 251: 41-51. <https://doi.org/10.1016/j.powtec.2013.10.023>
- [7] Xu, W., Yu, J., Wang, H. (2024). The influence of manganese slag on the properties of ultra-high-performance concrete. *Materials*, 17(2): 497. <https://doi.org/10.3390/ma17020497>
- [8] Nath, S.K., Kumar, S. (2016). Evaluation of the suitability of ground granulated silico-manganese slag in Portland slag cement. *Construction and Building Materials*, 125: 127-134. <https://doi.org/10.1016/j.conbuildmat.2016.08.025>
- [9] Chousidis, N., Rakanta, E., Ioannou, I., Batis, G. (2015). Anticorrosive effect of electrochemical manganese dioxide by-products in reinforced concrete. *Journal of Materials Science and Chemical Engineering*, 3(5): 9-20. <https://doi.org/10.4236/msce.2015.35002>

- [10] Pourchez, J., Grosseau, P., Ruot, B. (2009). Current understanding of cellulose ethers impact on the hydration of C₃A and C₃A-sulphate systems. *Cement and Concrete Research*, 39(8): 664-669. <https://doi.org/10.1016/j.cemconres.2009.05.009>
- [11] Zhou, C., Du, B., Wang, N., Chen, Z. (2014). Preparation and strength property of autoclaved bricks from electrolytic manganese residue. *Journal of Cleaner Production*, 84: 707-714. <https://doi.org/10.1016/j.jclepro.2014.01.052>
- [12] He, J., Sun, C., Hu, W., Ni, Z., Yin, X., Wang, X. (2024). Study on the effect of silica–Manganese slag mixing on the deterioration resistance of concrete under the action of salt freezing. *Buildings*, 14(9): 2684. <https://doi.org/10.3390/buildings14092684>
- [13] Ye, F., Cheng, H., Xiang, Y., Liu, S., Shi, W. (2023). Preparation of ceramic aggregate from electrolytic manganese slag and its application in concrete. *Inorganic Chemicals Industry*, 56(6): 127-132. <https://doi.org/10.19964/j.issn.1006-4990.2023-0489>
- [14] Cota, T.G., Cheloni, L.M.d.M.S., Guedes, J.J.M., Reis, É.L. (2023). Silico-manganese slag and its utilization into alkali-activated materials: A critical review. *Construction and Building Materials*, 399: 132589. <https://doi.org/10.1016/j.conbuildmat.2023.132589>
- [15] Rashiddadash, P., Ramezani-pour, A.A., Mahdikhani, M. (2014). Experimental investigation on flexural toughness of hybrid fiber reinforced concrete (HFRC) containing metakaolin and pumice. *Construction and Building Materials*, 51: 313-320. <https://doi.org/10.1016/j.conbuildmat.2013.10.087>
- [16] Shi, F., Pham, T.M., Hao, H., Hao, Y. (2020). Post-cracking behaviour of basalt and macro polypropylene hybrid fibre reinforced concrete with different compressive strengths. *Construction and Building Materials*, 262: 120108. <https://doi.org/10.1016/j.conbuildmat.2020.120108>
- [17] Shafei, B., Kazemian, M., Dopko, M., Najimi, M. (2021). State-of-the-art review of capabilities and limitations of polymer and glass fibers used for fiber-reinforced concrete. *Materials*, 14(2): 409. <https://doi.org/10.3390/ma14020409>
- [18] Abaean, R., Behbahani, H.P., Moslem, S.J. (2018). Effects of high temperatures on mechanical behavior of high strength concrete reinforced with high performance synthetic macro polypropylene (HPP) fibres. *Construction and Building Materials*, 165: 631-638. <https://doi.org/10.1016/j.conbuildmat.2018.01.064>
- [19] Gorji Azandariani, M., Vajdian, M., Asghari, K., Mehrabi, S. (2023). Mechanical properties of polyolefin and polypropylene fibers-reinforced concrete—An experimental study. *Composites Part C: Open Access*, 12: 100410. <https://doi.org/10.1016/j.jcomc.2023.100410>
- [20] Guo, H., Tao, J., Chen, Y., Li, D., Jia, B., Zhai, Y. (2019). Effect of steel and polypropylene fibers on the quasi-static and dynamic splitting tensile properties of high-strength concrete. *Construction and Building Materials*, 224: 504-514. <https://doi.org/10.1016/j.conbuildmat.2019.07.096>
- [21] Guler, S. (2018). The effect of polyamide fibers on the strength and toughness properties of structural lightweight aggregate concrete. *Construction and Building Materials*, 173: 394-402. <https://doi.org/10.1016/j.conbuildmat.2018.03.212>
- [22] Shen, D., Liu, X., Zeng, X., Zhao, X., Jiang, G. (2020). Effect of polypropylene plastic fibers length on cracking resistance of high performance concrete at early age. *Construction and Building Materials*, 244: 117874. <https://doi.org/10.1016/j.conbuildmat.2019.117874>
- [23] Castoldi, R.d.S., Souza, L.M.S.d., de Andrade Silva, F. (2019). Comparative study on the mechanical behavior and durability of polypropylene and sisal fiber reinforced concretes. *Construction and Building Materials*, 211: 617-628. <https://doi.org/10.1016/j.conbuildmat.2019.03.282>
- [24] Du, H.X., Qin, Y.X., Zhang, W., Zhang, N., Hao, X.Y. (2011). Mechanics performance of high-performance concrete with polypropylene fibers. *Applied Mechanics and Materials*, 99-100: 1233-1238. <https://doi.org/10.4028/www.scientific.net/AMM.99-100.1233>
- [25] Larsen, I.L., Thorstensen, R.T. (2020). The influence of steel fibres on compressive and tensile strength of ultra high performance concrete: A review. *Construction and Building Materials*, 256: 119459. <https://doi.org/10.1016/j.conbuildmat.2020.119459>
- [26] Shah, A.A., Ribakov, Y. (2011). Recent trends in steel fibered high-strength concrete. *Materials & Design*, 32(8-9): 4122-4151. <https://doi.org/10.1016/j.matdes.2011.03.030>
- [27] Shaikh, F.U.A., Luhar, S., Arel, H.Ş., Luhar, I. (2020). Performance evaluation of ultrahigh performance fibre reinforced concrete – A review. *Construction and Building Materials*, 232: 117152. <https://doi.org/10.1016/j.conbuildmat.2019.117152>
- [28] Hosseinzadeh, H., Salehi, A.M., Mehraein, M., Asadollahfardi, G. (2023). The effects of steel, polypropylene, and high-performance macro polypropylene fibers on mechanical properties and durability of high-strength concrete. *Construction and Building Materials*, 386: 131589. <https://doi.org/10.1016/j.conbuildmat.2023.131589>
- [29] Rambo, D.A.S., Silva, F.d.A., Toledo Filho, R.D. (2014). Mechanical behavior of hybrid steel-fiber self-consolidating concrete: Materials and structural aspects. *Materials & Design (1980-2015)*, 54: 32-42. <https://doi.org/10.1016/j.matdes.2013.08.014>
- [30] Yoo, D.Y., Kim, M.J., Kim, S.W., Park, J.J. (2017). Development of cost effective ultra-high-performance fiber-reinforced concrete using single and hybrid steel fibers. *Construction and Building Materials*, 150: 383-394. <https://doi.org/10.1016/j.conbuildmat.2017.06.018>
- [31] Yoo, D.Y., Kim, S.W., Park, J.J. (2017). Comparative flexural behavior of ultra-high-performance concrete reinforced with hybrid straight steel fibers. *Construction and Building Materials*, 132: 219-229. <https://doi.org/10.1016/j.conbuildmat.2016.11.104>
- [32] Pająk, M. (2016). Investigation on flexural properties of hybrid fibre reinforced self-compacting concrete. *Procedia Engineering*, 161: 121-126. <https://doi.org/10.1016/j.proeng.2016.08.508>
- [33] Pająk, M., Ponikiewski, T. (2017). Experimental investigation on hybrid steel fibers reinforced self-compacting concrete under flexure. *Procedia Engineering*, 193: 218-225. <https://doi.org/10.1016/j.proeng.2017.06.207>

- [34] Song, P.S., Hwang, S. (2004). Mechanical properties of high-strength steel fiber-reinforced concrete. *Construction and Building Materials*, 18(9): 669-673. <https://doi.org/10.1016/j.conbuildmat.2004.04.027>
- [35] Du, J.C., Kuo, M.F. (2011). Grey relational-regression analysis for hot mix asphalt design. *Construction and Building Materials*, 25(5): 2627-2634. <https://doi.org/10.1016/j.conbuildmat.2010.12.011>
- [36] Prusty, J.K., Pradhan, B. (2020). Multi-response optimization using Taguchi-Grey relational analysis for composition of fly ash-ground granulated blast furnace slag based geopolymer concrete. *Construction and Building Materials*, 241: 118049. <https://doi.org/10.1016/j.conbuildmat.2020.118049>
- [37] Liu, R.J., Ding, Q.J., Chen, P., Yang, G.Y. (2012). Durability of concrete made with manganese slag as supplementary cementitious materials. *Journal of Shanghai Jiaotong University (Science)*, 17(3): 345-349. <https://doi.org/10.1007/s12204-012-1284-y>
- [38] Taguchi G, Yokoyama Y. (1993). *Taguchi Methods: Design of Experiments*. ASI Press.
- [39] Li, J., Yang, F., Zhang, H., Wu, Z., Tian, Y., Hou, X., Xu, Y., Ren, J. (2020). Comparative analysis of different valve timing control methods for single-piston free piston expander-linear generator via an orthogonal experimental design. *Energy*, 195: 116966. <https://doi.org/10.1016/j.energy.2020.116966>
- [40] Deng, J.L. (1982). Control problems of grey systems. *Systems & Control Letters*, 1(5): 288-294. [https://doi.org/10.1016/S0167-6911\(82\)80025-X](https://doi.org/10.1016/S0167-6911(82)80025-X)
- [41] Ahmad, A., Khan, M.A., Akram, S., Faraz, M.I., Jaffery, S.H.I., Iqbal, T., Petru, J. (2024). Achieving sustainable machining of titanium grade 3 alloy through optimization using grey relational analysis (GRA). *Results in Engineering*, 23: 102355. <https://doi.org/10.1016/j.rineng.2024.102355>
- [42] Gerus-Gościewska, M., Gościewski, D. (2022). Grey relational analysis (GRA) as an effective method of research into social preferences in urban space planning. *Land*, 11(1): 102. <https://doi.org/10.3390/land11010102>